Original Manuscript

Journal of Industrial Textiles

Volume 52: 1–26

DOI: 10.1177/15280837221118063
journals.sagepub.com/home/jit
SAGE

Hydrophobic and oleophilic 3D weft-knitted spacer fabrics coated by silica aerogels with five different concentrations

Syed Rashedul Islam[1], Mohammed Kayes Patoary[1], Hewan Dawit Estifanos[2], Ishaq Lugoloobi[3], Alrayah HD Yousif[1], Jinhua Jiang[1] and Huiqi Shao[1]

Abstract

Silica aerogels were made from tetraethylorthosilicate by the sol-gel method and coated on the 3D weft-knitted spacer fabrics (WKSFs) to compare the interaction of the silica aerogel coating with five various concentrations. SEM, FTIR-ATR, surface roughness, surface energy, and BET analysis were used to observe and characterize the surface morphology, molecular interaction, surface changes, surface tension, and specific surface area of fabric samples or sorbents. Consequently, this study investigated the wettability,

[1]Shanghai Frontier Science Research Center for Modern Textiles, College of Textiles, Donghua University, Shanghai, China
[2]CAS Key Laboratory for Nano-bionics Interface, Suzhou Institute of Nano-tech and Nano-bionics, Chinese Academy of Science, University of Science and Technology, Suzhou, China
[3]CAS Key Laboratory of Soft Matter Chemistry and School of Chemistry and Materials Science, University of Science and Technology of China, Hefei, China

Corresponding authors:
Jinhua Jiang, Shanghai Frontier Science Research Center for Modern Textiles, College of Textiles, Donghua University, Room No. 4013, College of Textiles, Donghua University, 2999, North Renmin Rd, Songjiang District, Shanghai, 201620, China.
Email: jiangjinhua@dhu.edu.cn

Syed Rashedul Islam, Shanghai Frontier Science Research Center for Modern Textiles, College of Textiles, Donghua University, Room No. 4013, College of Textiles, Donghua University, 2999, North Renmin Rd, Songjiang District, Shanghai, 201620, China.
Email: sri060791@gmail.com

oil absorption capacity, oil retention capacity, and reusability of untreated and treated 3D WKSF sorbents. The outcomes exposed the excellent hydrophobic and oleophilic properties of all treated 3D WKSF sorbents, showing a greater water contact angle of 145.1 ± 0.42°, and an oil absorption and retention capacity of (7.87 ± 0.09 g/g and 7.53 ± 0.06 g/g) and (89.98 ± 0.79% and 92.48 ± 0.56%) for vegetable oil and engine oil, respectively, with notable reusability, most particularly for sorbent 5, due to the higher silica aerogel add-on %, pore diameter, and pore volume. The findings verified that the chemical composition and fabric structure played an important role in the tremendous hydrophobic and oleophilic behavior. The statistical study on specific surface area, pore diameter, pore volume, surface roughness, water contact angle, oil contact angle, oil absorption capacity, and oil retention capacity also revealed that treated fabrics performed significantly ($p < 0.05$) in hydrophobic and oleophilic features at the 0.05 level. Hence, these fabrics can be used in industrial usages that need hydrophobic and oleophilic qualities.

Keywords
3D spacer fabrics, silica aerogels add-on %, oil absorption, oil retention, reusability

Introduction

Oil has been a part of the environment for a number of years due to the rapid expansion of oil manufacturing, exploration, transport, and storage.[1–5] Oil spills have received more attention recently among contaminated occurrences as a result of significant environmental concerns and economic losses that have put human health at risk.[6–11] These spills are caused by production, exploration, transport, stowing, usage, equipment failures, operational failures, and natural disasters. Oil spills pose a serious environmental hazard to society when they occur on the land, in the river, or in the ocean.[12,13] Moreover, cleaning the water and recovering the oil quickly after the leak is a great challenge in this situation. As a result, a variety of technologies for cleaning and recycling spilled oil has been implemented. Among these methods, mechanical separation, chemical separation, and biological remediation are only a few of the advanced cleanup methods developed and used in oily water remediation.[14–17] Mechanical oil recovery using sorbent materials is one of the most promising and feasible technologies in maritime oil-spill response among the existing methods.[18,19]

Hydrophobicity, oleophilicity, absorption capability, resilience, better oil/water separation, and reusability are all desirable qualities in an oil sorbent material.[20–22] Due to unique advantages such as outstanding chemical and mechanical competencies, as well as easy processing, synthetic polymer materials such as polyester (PET) are now commonly employed as oil sorbents.[23–25] PET also possesses hydrophobic and oleophilic properties, making it a viable material for oil spill remediation.[26–28] However, this material has significant limitations (chemical structure, strong ester linkage, and surface chemistry)

that cause it to degrade very slowly, which is assumed to be the primary source of the phenomena recognized as white contamination.[29–31]

Because of the particular molecular structure, wettability, oleophilicity, lightweight, inferior density, superior porosity, and heat resistance, silica aerogels (SAs) stand out of all aerogels, i.e., cellulosic, phenol, carbon, graphene, inorganic, etc.[32–37] Few scientists have used the methyltrimethoxysilane and polydimethylsiloxane precursor to form SAs and oil-absorbing sponges.[38,39] Some researchers have also studied the elastic and oleophilic tetraethylorthosilicate (TEOS)-based and methyltrimethoxysilane (MTES)-based silica aerogels for preparing hydrophobic and oil-absorbing sorbents.[40,41] Materials with fluorinated alkylsilane and polyaniline, polyacrylamide hydrogel synthetization, nitric acid solution, cross-linking onto polyester fabric via UV-initiated polymerization, and lignin incorporation in polypropylene via thermally induced phase separation are also most popular examples.[42–47] The majority of these approaches have weaknesses, such as costly, less durable, difficult processes, and time-consuming preparations.[48,49] As a result, the search for resilient and stretchable textile materials with excellent water-repelling and oil-absorbing characteristics still continues.

Two outer layers of elastic yarn (top and bottom layers) and one middle layer of spacer yarn are used to make the 3D WKSFs.[50] Oleophilic, hydrophobic, physiological, mechanical, thermal, bending, elastic, and compression properties of these fabrics make them multi-functional materials.[51–55] Furthermore, they are strong, durable, recyclable, and reusable.[56,57] Minor proportions of nano and microparticle fillers have enhanced the functional properties of 3D WKSFs; nevertheless, their water-repelling and oil-absorbing features are identically limited.[58–62] By using several precursors, co-precursors, and silylating agents with SAs coating, the surface roughness, and specific surface area can be increased, and the surface energy can be decreased, potentially improving the hydrophobicity and oleophilicity of 3D WKSFs.[63–67] Nowadays, the production of hydrophobic and oleophilic surfaces using the sol-gel method has received much interest and has been used widely in many researches.[68,69]

No research work has been found between different concentrations of SAs and 3D WKSFs for water-repelling and oil-absorbing materials with reusability properties. As a result, five different concentrations of silica aerogels are made from tetraethylorthosilicate using sol-gel technology to introduce a new type of hydrophobic and oleophilic 3D WKSF sorbent in the current work. Moreover, Scanning electron microscopy (SEM), Brunauer–Emmet–Teller (BET), Fourier transform infrared spectroscopy–attenuated total reflection (FTIR-ATR), surface wettability, surface roughness (SR), and surface energy (SE) tests are used to evaluate the effect of SAs on the hydrophobic and oleophilic characteristics with the reusability of treated and untreated 3D WKSFs. Thus, in this work, 3D WKSF sorbents with SAs coating are explored as a new potential source for water-repelling (hydrophobic) and oil-absorbing (oleophilic) materials.

Experimental works

Materials

3D WKSFs (92% polyester and 8% spandex) were collected from Tianbin Textile Co. Ltd., Changshu, China. These fabrics were made on a circular knitting machine of gauge 28. The spacer fabrics were delivered with a similar yarn count of 75D for both the top layer and bottom layer. The yarn count of the middle layer of 3D WKSFs was 40D. The thickness and GSM (Gram per square meter) of the samples were 3 mm and 350 gm^{-2}, respectively. Wales and courses of the sample were 47 in^{-1} and 60 in^{-1}, individually. The stitch density and fabric density of fabric were 1.58 in^{-1} and 117 kgm^{-3}, respectively. The porosity (%) and spacer yarn arrangement angle of fabric were 87.54% and 79.96°, separately. Tetraethylorthosilicate (>99%, TEOS) and N-hexane (>99%) were purchased from National Drug Group Chemical Reagent "Co. Ltd." and Yangyuan Chemical Texnology "Co. Ltd.". Ethyl alcohol (99%, E_tOH), N, N-dimethyl-formamide (>98%, DMF), Hydrochloric acid (37%, HCl), and Ammonia (25%, NH_4OH) were procured from Shanghai Union Chemical Industry "Co. Ltd.", Shanghai Lingfeng Chemical Reagent "Co. Ltd.", Algae Group Chemical Reagent "Co. Ltd.", and Shanghai Macklin Biochemical "Co. Ltd.". Hexamethyldisilazane (≥99%, HMDS) was bought from Shanghai Code Group Chemical Brake "Co. Ltd.". All the chemicals and reagents were applied without any further rectification. Besides, two kinds of oils (vegetable oil and engine oil) were used for oleophilic tests. The surface tension, density, and viscosity of vegetable oil and engine oil were (32.45 ± 0.30 $mN.m^{-1}$, 0.89 ± 0.20 $g.cm^{-3}$, and 62.7 ± 12.50 mPa.s) and (29.7 ± 0.50 $mN.m^{-1}$, 0.85 ± 0.10 $g.cm^{-3}$, and 233.5 ± 15.70 mPa.s), respectively.

Silica sol preparation

The silica sol-gel procedure consisted of two steps: acid-catalyzed tetraethylorthosilicate ($C_8H_{20}O_4Si$) hydrolysis followed by base-catalyzed gelation.[35] For preparing the five different concentrations of silica aerogels (SAs 1, SAs 2, SAs 3, SAs 4, and SAs 5), certain amounts of $C_8H_{20}O_4Si$ were dissolved in certain amounts of Ethyl alcohol (C_2H_5OH). A magnetic stirrer was used to agitate this mixture for 0.5 h at 400 r/min to generate a homogenous solution. For each concentration, 28.50 mL of HCl was dissolved in 95.50 mL of H_2O to make the acid catalyst solution. After that, (HCl/H_2O) mixture was dropped slowly into the (Tetraethylorthosilicate/Ethyl alcohol) solution, which was magnetically stirred for 1 h at 60°C. Then, with magnetic stirring for 0.5 h, 32.50 mL of NH_4OH was added to the (Tetraethylorthosilicate/Ethyl alcohol) solution. Similarly, 32.50 mL of DMF was added to the silica sols to create a homogeneous nano-porous gel structure. Likewise, magnetic stirring was used to dissolve 32.50 mL of HMDS in the gel solution for 2 h at 60°C. Five different concentrations of silica aerogels were prepared in this research to investigate the hydrophobic and oleophilic properties of 3D weft-knitted spacer fabrics, as listed in Table 1.

Coating on 3D weft-knitted spacer fabrics (WKSFs) with silica aerogels (SAs)

Samples of 3D WKSFs were cut into 35 cm^2 and soaked in silica sol-gel for 15 min.[51] The samples were then solidified and placed in a tightly sealed container. After forming the gelled layer on the 3D WKSFs samples for 20 min, the wet-gelled samples were kept at 25°C for 24 h to secure the silica aerogel network structures on the samples. After that, the wet-gelled 3D WKSFs were washed in ethanol for 8 h. This ethanol washing process was repeated 3 times with the exchange of n-hexane each time. To eliminate the ethanol-containing solution, the wet-gelled layers of 3D WKSFs were washed with n-hexane for 8 h. In the end, these 3D WKSF samples were dried for 5 h in an oven at 40°C, 60°C, and 100°C, respectively. The fabrication steps of hydrophobic and oleophilic 3D WKSF sorbent by SAs coating were shown in Figure 1.

Add-on % of silica aerogels

The untreated and treated spacer fabric samples were dried for 1 h at 107°C. The add-on % of silica aerogels on 3D WKSF was calculated by equation (1),[51] as shown in Table 2.

$$Silica\ aerogels\ add-on\ \% = \frac{W_t - W_u}{W_u} \times 100 \quad (1)$$

where W_u is the weight of untreated samples (UTS) in Gram and W_t is the weight of treated samples (TS) in Gram.

SEM analysis

A Flex-SEM 1000 (scanning electron microscopy, 10.00 KV × 200SE, SU1000, Hitachi Ltd. Japan) was used to observe the surface morphology changes by the SiO_2 aerogel coating. Before the investigation, all 3D WKSF samples were coated with the gold coating by the vacuum falter coater.

Table 1. Five different concentrations of silica aerogels (SAs).

Chemicals	SAs 1 (ml)	SAs 2 (ml)	SAs 3 (ml)	SAs 4 (ml)	SAs 5 (ml)
TEOS	80.50	90.50	100.50	110.50	120.50
EtOH	698	688	678	668	658
HCl	28.50	28.50	28.50	28.50	28.50
H_2O	95.50	95.50	95.50	95.50	95.50
NH_4OH	32.50	32.50	32.50	32.50	32.50
DMF	32.50	32.50	32.50	32.50	32.50
HMDS	32.50	32.50	32.50	32.50	32.50

FTIR analysis

A Nicolet TM 5700 FT-IR spectrometer, America (Fourier transform infrared spectroscopy-FTIR) for the microstructure of 3D WKSFs was used to characterize the surface changes influenced by the SiO_2 aerogel coating. The spectra were made using the ATR (attenuated total reflection technique) in the range of 400–5000 cm^{-1}. The FTIR-ATR test was used in 64 scans with a resolution of 8 cm^{-1}.

BET specific surface test

The Brunauer–Emmet–Teller (BET) specific surface area of the 3D weft-knitted fabric samples was performed by N_2-adsorption experiments with an ASAP2010 (Micromeritics, U.S.A). Before beginning the test, the 3D weft-knitted spacer fabric samples were degassed at 150°C. BET specific surface test was used to characterize the specific surface area, pore diameter, and pore volume of WKSFs.[36]

Surface energy test

The Owens-Wendt-Rabel-Kaelble (OWRK) method was used to measure the surface energy of 3D WKSF sorbents. The liquids used in this experiment were H_2O (water), $C_2H_6O_2$ (ethylene glycol), and C_2H_5OH (ethanol). The temperature for the test was kept

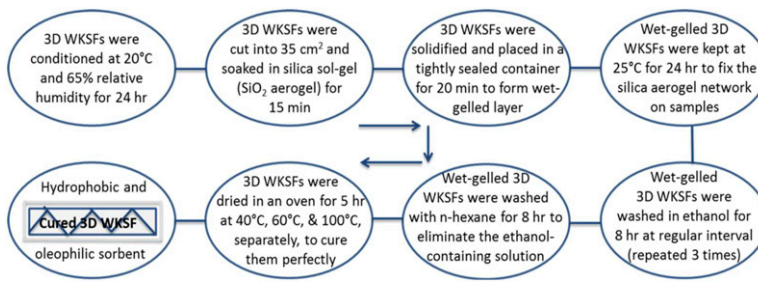

Figure 1. The fabrication steps of hydrophobic and oleophilic 3D weft-knitted spacer fabric sorbent by silica aerogels coating.

Table 2. The add-on % of silica aerogels on treated 3D WKSFs.

Samples	Add-on % of silica aerogels	Coefficient of variation (CV %)
TS 1	36.85 ± 0.29	0.79
TS 2	37.32 ± 0.28	0.75
TS 3	37.74 ± 0.25	0.66
TS 4	38.27 ± 0.22	0.57
TS 5	38.89 ± 0.18	0.46

TS: treated sample.

Table 3. The surface tension (ST) characteristics of liquid solution for samples.

Liquid solution	PC $mN.m^{-1}$	DC $mN.m^{-1}$	ST $mN.m^{-1}$
H_2O	52.20 ± 0.40	19.90 ± 0.10	72.10 ± 0.50
$C_2H_6O_2$	29.00 ± 0.39	19.00 ± 0.28	48.00 ± 0.67
C_2H_5OH	4.60 ± 0.21	17.50 ± 0.25	22.10 ± 0.46

PC: polar component; DC: dispersion component; ST: surface tension.

at 20°C. The surface tension (ST) or surface energy (SE) of various liquids was presented in Table 3.

Surface roughness test

The Kawabata Evaluation System for 3D WKSFs was used to determine the surface roughness (KES-FB-4, Japan). For this investigation, 3D WKSFs samples were cut into 20 cm^2. To attain an average value, each test was repeated thrice. Before measurement performance testing, all 3D WKSF samples were conditioned for 24 h at 20°C and 65% relative humidity.

Contact angle (CA) test

Optical video contact angle equipment (Model OCA 40, Germany) was used to calculate the water contact angle (WCA) or surface wettability. After placing a 5 μL water drop on 3D WKSF samples, the WCA was measured for 60 s. For each sample, the contact angles displayed were the average of approximations from five different places.

Oleophilic test

The oil absorption capacity was determined using the ASTM F 716–09 standard.[18] The fabric sorbent (3 cm^2) was submerged in 150 mL of oil for 15 min to captivate the oil up until no discernible weight change was observed. The 3D WKSF sorbent was replaced, positioned on wire mesh, and endorsed to drain to eliminate any remaining oil. By following the average of 3 and 5 times repetition, the oil absorption capacity and oil retention capacity were examined. The temperature of the test was kept constant at 22 ± 2°C. According to equations (2) and (3), the oil absorption capacity and oil retention capacity were computed.[70]

$$\text{Oil absorption capacity} = (m_2 - m_1)/m_1 \tag{2}$$

$$\text{Oil retention capacity} = (m_3 - m_1)/(m_2 - m_1) \times 100 \tag{3}$$

where m_1 = the weight of the dried 3D WKSF sorbent before absorption in Gram, m_2 = the total weight of wetted 3D WKSF sorbent after oil draining out for 1 min in Gram, and m_3 = the weight of wetted 3D WKSF sorbent after 24 h dripping in Gram.

Statistical analysis

The data in this study were analyzed using statistical analysis of difference with (two pair-wise t-tests) dissimilar comparisons. Through a 95% confidence interval, a p-value of 0.00 ($p < 0.05$) was found to be a statistically significant variance.

Results and discussion

Morphological properties of the 3D weft-knitted spacer fabrics

The surface particle morphology and physical microstructure of the untreated and treated 3D weft-knitted spacer fabrics by silica aerogels were observed through the SEM analysis, as exposed in Figure 2. Figure 2(a) presented the untreated samples (UTS) of spacer fabric surface whereas Figure 2(b) to (f) displayed the compressed surface morphology and incessant structure of the treated samples (TS). On the surface of the treated samples, the silica aerogels (SAs 1, SAs 2, SAs 3, SAs 4, and SAs 5) created an alike, nanoporous, and well-formed linkage. The substrate surface improved the homogeneous coating of all treated fabrics after these were coated with silica aerogels. The surface of silica aerogels-treated spacer fabrics was thicker than that of untreated spacer fabrics. The spacer fabric's surface became severe and harsh as a result of the silica aerogel coating. Moreover, the SiO_2 grid was present in the fabric structure of coated or treated spacer fabrics. In the spaces between the fibers of treated 3D WKSFs, a number of crusts and huge interphase

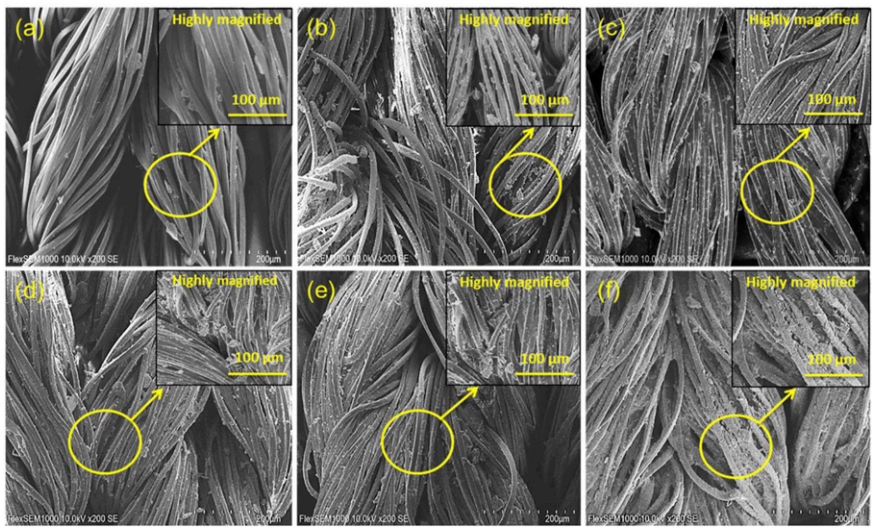

Figure 2. SEM images (scale bars 200 µm) of (a) untreated and (b–f) treated samples with silica aerogels.

bridges were also discovered. Likewise, there were some friezes on the treated 3D WKSF surfaces.

Among all the treated spacer fabric samples, TS 5 (f) had the most SiO_2 aerogel particles (add-on %) on its surface. Besides, it possessed a higher pore diameter and pore volume. In comparison to TS 1 (b), TS 2 (c), TS 3 (d), and TS 4(e), TS 5 (f) generated the highest water contact angle (WCA) due to the highest specific surface area, highest surface roughness, and the lowest surface energy. The lowest WCA was found in TS 1 (b), which had the least amount of silica aerogel particles (add-on %) on its surface. Furthermore, it had the lowest specific surface area, lowest surface roughness, and the highest surface energy. As a result, it was smoother than the other four treated samples. The existence of Si-O-Si network constructions in the treated 3D WKSFs offered thermodynamic motion from inside to outside and the creation of a homogenous SiO_2 aerogel coating induced constant material distribution on the fabric surface, resulting in decreased surface energy and increased surface roughness, thus, enhanced the hydrophobic and oleophilic properties of the treated samples.[63,71,72]

Chemical interaction of untreated and treated 3D weft-knitted spacer fabrics

The FTIR spectra of untreated and treated 3D weft-knitted spacer fabric samples (UTS and (TS 1, TS 2, TS 3, TS 4, and TS 5)) were shown in Figure 3. The accessibility of a specific functional group was indicated by all individual absorption peaks. The stretching and

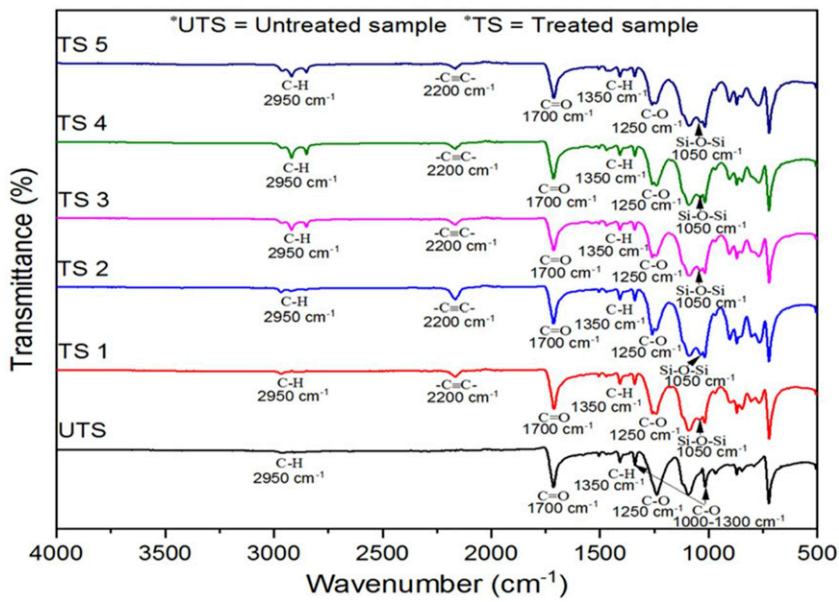

Figure 3. FTIR spectra of untreated and treated 3D weft-knitted spacer fabrics.

bending of C-O bonds caused the absorption peak to appear at around 1000–1300 cm^{-1}. Both untreated and treated spacer fabric samples contained it. Furthermore, the formation of a nano-porous SiO_2 linkage structure on the treated samples was confirmed by the absorption peak at 1050 cm^{-1}, which was caused by the imbalanced stretching and vibration of Si-O-Si bonds. Furthermore, the peaks at 1050 cm^{-1} triggered the spectra of the untreated and treated samples to differ. The stretching and bending of C–H bonds resulted in an absorption band at around 1350 cm^{-1} and 2950 cm^{-1} in both untreated and treated samples. All the fabric samples had C=O groups in their structures, according to the strong peak at 1700 cm^{-1}. The asymmetric stretching of -C≡C- bonds in the treated samples produced a new peak at 2200 cm^{-1}. Moreover, the existence of Si-O-Si bonds in the spectrum increased the treated samples' hydrophobic and oleophilic characteristics.

BET specific surface area (SSA) test of 3D weft-knitted spacer fabrics

The specific surface area, pore diameter, and pore volume of treated 3D weft-knitted spacer fabric samples (TS 1, TS 2, TS 3, TS 4, and TS 5) were perceived higher than their corresponding untreated weft-knitted spacer fabric samples (UTS), as shown in Table 4. The BET specific surface area of treated samples (TS 1, TS 2, TS 3, TS 4, and TS 5) was 4.62 times, 4.66 times, 4.71 times, 4.76 times, and 4.81 times higher than that of their untreated samples (UTS). The pore diameter of TS 1, TS 2, TS 3, TS 4, and TS five was 1.25 times, 1.26 times, 1.27 times, 1.28 times, and 1.29 times higher than their corresponding UTS. Similarly, the pore volume of TS 1, TS 2, TS 3, TS 4, and TS 5 was 6.8 times, 7.47 times, 8.27 times, 9.13 times, and 10.00 times higher than UTS. The upgrading of specific surface area, pore diameter, and pore volume was due to the surface changes by silica aerogels coating. Sample (TS 5) exhibited a better specific surface area, pore diameter, and pore volume among all samples due to the greater add-on % of silica aerogels in fabric structure after silica aerogels coating. The higher specific surface area directed the better surface roughness of treated samples and that was also confirmed by SEM analysis and surface roughness test. Therefore, it indicated the better hydrophobic and oleophilic properties of treated samples.

Table 4. The BET outcomes of untreated and treated 3D weft-knitted spacer fabrics.

Samples	Specific surface areas (m^2g^{-1})	CV (%)	Pore diameter (Nm)	CV (%)	Pore volume (cm^3g^{-1})	CV (%)
UTS	1.131 ± 0.02	1.77	3.055 ± 0.04	1.31	0.0015 ± 0.0001	6.67
TS 1	5.225 ± 0.05	0.96	3.812 ± 0.04	1.05	0.0102 ± 0.0002	1.96
TS 2	5.274 ± 0.04	0.76	3.841 ± 0.03	0.78	0.0112 ± 0.0002	1.79
TS 3	5.326 ± 0.04	0.75	3.875 ± 0.03	0.77	0.0124 ± 0.0002	1.61
TS 4	5.378 ± 0.03	0.56	3.907 ± 0.02	0.51	0.0137 ± 0.0002	1.46
TS 5	5.435 ± 0.03	0.55	3.945 ± 0.02	0.51	0.0150 ± 0.0002	1.33

Table 5. The WCA, oil contact angle (OCA), and surface energy of UTS and TS 3D WKSFs.

Samples	Contact angle (°)			Surface energy ($mN.m^{-1}$)		
	Water	VO	EO	DC	PC	Total
UTS	90.7 ± 1.37	43.4 ± 0.69	38.2 ± 0.60	29.92 ± 0.39	4.41 ± 0.21	34.33 ± 0.60
TS 1	138.7 ± 1.12	27.6 ± 0.50	25.8 ± 0.42	21.18 ± 0.33	2.67 ± 0.22	23.85 ± 0.55
TS 2	139.3 ± 0.88	26.5 ± 0.47	24.7 ± 0.35	20.52 ± 0.23	2.45 ± 0.14	22.97 ± 0.37
TS 3	140.8 ± 0.72	25.7 ± 0.44	24.2 ± 0.32	19.91 ± 0.17	2.29 ± 0.10	22.20 ± 0.27
TS 4	142.3 ± 0.54	24.6 ± 0.39	23.9 ± 0.29	19.37 ± 0.13	2.16 ± 0.12	21.53 ± 0.25
TS 5	145.1 ± 0.42	24.1 ± 0.32	23.5 ± 0.25	18.95 ± 0.11	2.01 ± 0.08	20.96 ± 0.19

VO: vegetable oil; EO: engine oil; PC: polar component; DC: dispersion component.

Surface energy (SE) test of 3D weft-knitted spacer fabrics

The surface energy, water contact angle, vegetable oil contact angle, and engine oil contact angle of untreated samples (UTS) and treated samples (TS 1, TS 2, TS 3, TS 4, and TS 5) were displayed in Table 5. All the coated fabric samples showed a noticeable change in surface energy, water contact angle, vegetable oil contact angle, and engine oil contact angle. After SAs coating, the surface energy and oil contact angle of treated samples (TS 1, TS 2, TS 3, TS 4, and TS 5) decreased and the water contact angle increased dramatically. The treated sample (TS 5) had a lower surface energy, ranging from 34.33 ± 0.60 $mN.m^{-1}$ to 20.96 ± 0.19 $mN.m^{-1}$, which was close to the surface energy of oils (20–30) $mN.m^{-1}$ but much lower the surface energy of water (72 ± 0.50 $mN.m^{-1}$), resulting in the treated samples' tremendous hydrophobicity and a higher water contact angle of 145.1 ± 0.42°. Other treated samples (TS 1, TS 2, TS 3, and TS 4) had a relatively larger surface energy; though, they had also improved hydrophobicity, with relatively lower water contact angles. Moreover, untreated samples (UTS) had a comparatively largest surface energy with the lowest water contact angles. Besides, when associating the compositions of surface energy, significant differences were observed in the treated samples. The ratio of dispersion component to polar component in the treated sample (TS 5) was 9.43, followed by 8.97, 8.69, 8.38, 7.93, and 6.78 for TS 4, TS 3, TS 2, TS 1, and UTS, individually. Thus, fabric sorbents' ability to absorb oil was aided by the dispersion and polar composition of surface energy.

Surface roughness (SR) test of 3D weft-knitted spacer fabrics

The surface roughness of untreated samples (UTS) and treated samples (TS 1, TS 2, TS 3, TS 4, and TS 5) of 3D weft-knitted spacer fabric samples (WKSFs) was exhibited in Figure 4. Untreated 3D WKSFs had a surface roughness of 0.82 ± 0.02 μm, whereas treated 3D WKSFs (TS 1, TS 2, TS 3, TS 4, and TS 5) had a surface roughness of 0.99 ± 0.02 μm, 1.06 ± 0.02 μm, 1.10 ± 0.01 μm, 1.13 ± 0.01 μm, and 1.16 ± 0.01 μm, respectively, which was 1.21 times, 1.29 times, 1.34 times, 1.38 times, and 1.41 times better than their imitating UTS. After coating, the surface roughness of treated samples

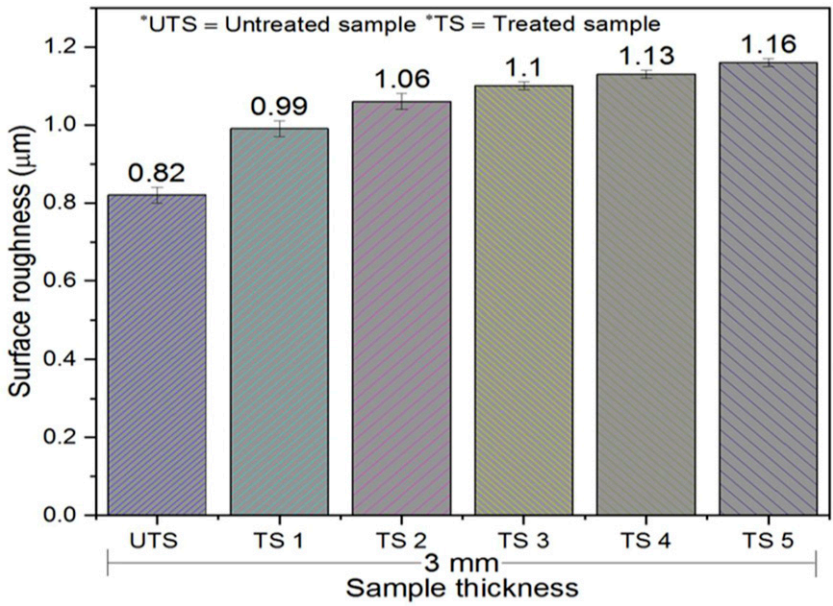

Figure 4. Surface roughness of untreated and treated spacer fabric samples.

improved by 20.73%, 29.27%, 34.15%, 37.80%, and 41.46%, respectively. This was due to the presence of stubs and burls in the treated spacer fabric structures. Moreover, the rougher the surface of the samples, the higher the water contact angle. The treated sample (TS 5) exposed a superior water contact angle and inferior oil contact angle owing to its higher surface roughness and higher specific surface area among all the samples that generated an excellent hydrophobic and oleophilic surface to the water and oil.

Hydrophobic or water contact angle test of 3D weft-knitted spacer fabrics

The water contact angle (WCA) of untreated and treated 3D weft-knitted spacer fabrics was depicted in Figure 5. The treated samples (TS 1, TS 2, TS 3, TS 4, and TS 5) had a larger WCA than the untreated samples (UTS) of weft-knitted spacer fabrics. Static WCA was performed on the untreated and treated fabric samples by dropping 5 μL water drops on various locations on the fabric surfaces. The water drop stayed on the treated fabric sample surface for a prolonged time with greater contact angles, specifying the treated samples' superior hydrophobicity (see, Figure S1, Supplementary Supporting file). After coating with silica aerogels, the WCA upgraded from 90.7 ± 1.37° to 138.7 ± 1.12°, 139.3 ± 0.88°, 140.8 ± 0.72°, 142.3 ± 0.54°, and 145.1 ± 0.42°, respectively, for treated samples (TS 1, TS 2, TS 3, TS 4, and TS 5). Moreover, the WCA of TS 1, TS 2, TS 3, TS 4, and TS five was 1.53 times, 1.54 times, 1.55 times, 1.57 times, and 1.60 times larger than their following UTS. The WCA of five treated samples improved by 52.92%,

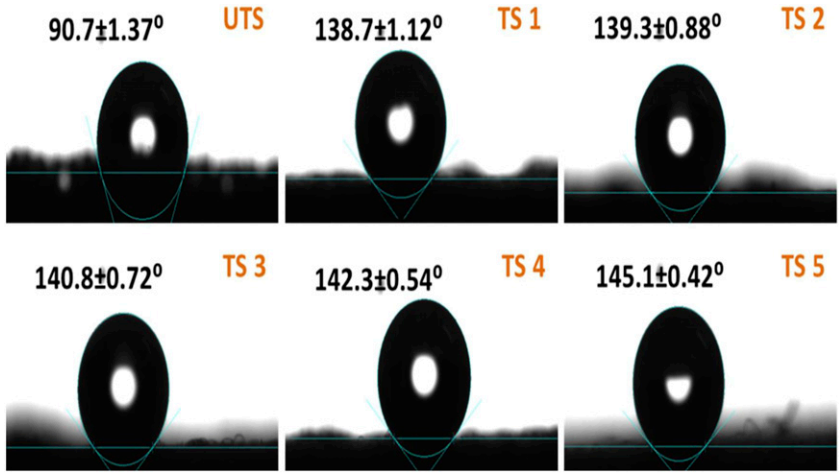

Figure 5. The water contact angle of untreated and treated 3D spacer fabric samples.

53.58%, 55.24%, 56.89%, and 59.98%, after coating, correspondingly. This was due to the presence of crusts and massive interphase bridges in the gaps of the treated samples. Besides, several burls and stubs with greater roughness were seen on all treated samples' surfaces. TS five showed the most projected WCA values, followed by TS 4, TS 3, TS 2, and TS 1, because it detained the greater SiO_2 aerogel add-on % in the spacer fabric structures after silica aerogel coating, even though every treated sample enhanced the WCA significantly. The greater the silica aerogel add-on % and specific surface area of samples, the higher the water contact angles of treated samples.

Oleophilic features of 3D weft-knitted spacer fabrics

The oleophilic (oil absorption and retention) test was conducted for untreated and treated 3D weft-knitted spacer fabrics for two different pure oils (vegetable and engine), as presented in Figure 6. The vegetable oil absorption capacity enhanced from 5.48 ± 0.18 g/g to 7.01 ± 0.15 g/g, 7.21 ± 0.14 g/g, 7.42 ± 0.12 g/g, 7.64 ± 0.11 g/g, and 7.87 ± 0.09 g/g after SAs coating for TS 1, TS 2, TS 3, TS 4, and TS 5, respectively. Similarly, the engine oil absorption capacity also improved from 5.25 ± 0.15 g/g to 6.63 ± 0.12 g/g, 6.83 ± 0.10 g/g, 7.05 ± 0.09 g/g, 7.28 ± 0.08 g/g, and 7.53 ± 0.06 g/g for TS 1, TS 2, TS 3, TS 4, and TS 5, respectively. Consequently, there was a noteworthy development in the oil absorption capacity of all treated 3D WKSFs. The enhancing rates of vegetable oil absorption of five treated samples were 27.92%, 31.57%, 35.40%, 39.42%, and 43.61%, respectively, whereas, the enhancing rates of engine oil absorption capacity of the same samples were 26.29%, 30.10%, 34.29%, 38.67%, and 43.43%, respectively. The results showed that the vegetable oil absorption capacity of both untreated and treated samples was greater than that of engine oil. The lower viscosity of vegetable oil allowed it to

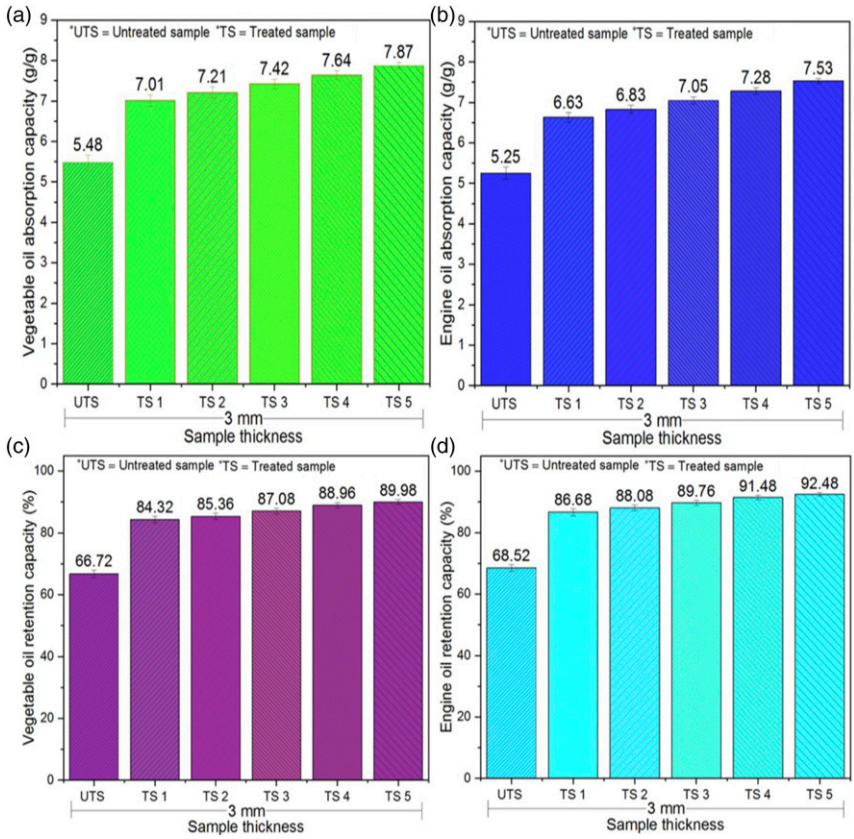

Figure 6. Oil absorption (a, b) and retention (c, d) capacity of 3D spacer fabric sorbents.

quickly flow into a capillary network of 3D WKSF sorbents. On the other hand, the higher viscosity of engine oil had a considerable impact on the capillary system during absorption. Furthermore, vegetable oil had a higher density and surface tension than engine oil. In comparison to engine oil, fabric sorbents with more nano-porous SiO_2 aerogel particles captivated more vegetable oil. TS 5 had the highest oil absorption capacity among all the treated 3D WKSF samples (TS 5 > TS 4 > TS 3 > TS 2 > TS 1), for both oils. This was owing to the bigger silica aerogel add-on %, larger pore diameter, and larger pore volume. By employing the high viscosity of engine oil, small pore size had a major impact on the capillary process, which became congested. Darcy's law assumed that when oil ensured a high viscosity, small pores would be occluded, and thus, oil absorption capacity would be reduced.[73] The oil absorption capacity increased as the silica aerogel add-on %, pore diameter, and pore volume increased. Hence, the hydrophobic connection and van der walls force between the 3D sorbents and the oils resulted in a greater oil pickup ability.

On the other hand, the vegetable oil retention capacity enhanced from 66.72 ± 1.19% to 84.32 ± 1.09%, 85.36 ± 1.04%, 87.08 ± 0.96%, 88.96 ± 0.91%, and 89.98 ± 0.79% after

SAs coating for TS 1, TS 2, TS 3, TS 4, and TS 5, respectively. Similarly, the engine oil retention capacity also improved from 68.52 ± 1.11% to 86.68 ± 1.16%, 88.08 ± 0.94%, 89.76 ± 0.85%, 91.48 ± 0.77%, and 92.48 ± 0.56% for TS 1, TS 2, TS 3, TS 4, and TS 5, respectively. Hence, there was a substantial enhancement in the oil retention capacity of all studied treated 3D WKSFs. The increasing rates of vegetable oil retention capacity of five treated samples were 26.38%, 27.94%, 30.52%, 33.33%, and 34.86%, respectively, whereas, the increasing rates of engine oil retention capacity of the same samples were 26.5%, 28.55%, 31%, 33.51%, and 34.97%, respectively. According to the results, the engine oil retention capacity was higher than the vegetable oil for both untreated and treated 3D WKSF sorbents. The soaked oil was further aided by the pore size diameter and viscosity of the oil. The lowest viscosity of vegetable oil drains more quickly. This aided the system's evenness quicker, as soybean oil had a higher inclination to stay within the sorbent than engine oil. The higher the add-on % of silica aerogels, pore diameter, and pore volume, the greater the oil retention capacity of 3D WKSFs. As a result, this technique was effective in the development of oil sorbents with improved oil absorption properties.

Oil absorption mechanism of 3D weft-knitted spacer fabrics

To further demonstrate, the oil absorption mechanism for fabric sorbents was explained by one or more of the mechanisms, or by a combination of mechanisms. The first one was a porous surface with low surface free energy, which allowed oil easily to wet it. Due to the hydrophobic interaction and van der walls force, the absorption process between the fabric sorbents and the oils resulted in a greater oil pick up. The second one was a capillary action, which was a surface phenomenon in which oil flowed freely into small areas. The lower surface energy, computed using the (OWRK) technique, was found to be in the range of (20.96 ± 0.19–34.33 ± 0.60) $mN.m^{-1}$, close to the surface energy of oils (20–30) $mN.m^{-1}$ but much lower that of water (72 $mN.m^{-1}$), leading to the sorbents' hydrophobicity, with a water contact angle of up to145.1 ± 0.42°. Hence, the 3D weft-knitted spacer fabrics' oil absorption capacity mainly depended on oil properties, fabric properties, nanoporous SiO_2 aerogel properties, and spaces inside and between fibers and fabrics.

The relationships among water contact angle, oil absorption, and retention capacity

Oil absorption capability and oil retention capacity of 3D weft-knitted spacer fabric sorbents were stated by the water contact angle (WCA). The water contact angle, oil absorption capacity, and oil retention capacity curvatures had been demonstrated in Figure 7 by growing the direction of WCA of the studied untreated and treated 3D weft-knitted spacer fabrics (WKSFs). When the water contact angle developed from 90.7 ± 1.37° to 145.1 ± 0.42°, the oil absorption capacity and oil retention capacity of untreated and treated 3D spacer fabrics altered from (5.48 ± 0.18 g/g to 7.87 ± 0.09 g/g) and (66.72 ± 1.19% to 89.98 ± 0.79%) for vegetable oil and (5.25 ± 0.15 g/g to 7.53 ± 0.06 g/g) and (68.52 ± 1.11% to 92.48 ± 0.56%) for engine oil, similarly. This indicated that 3D WKSFs

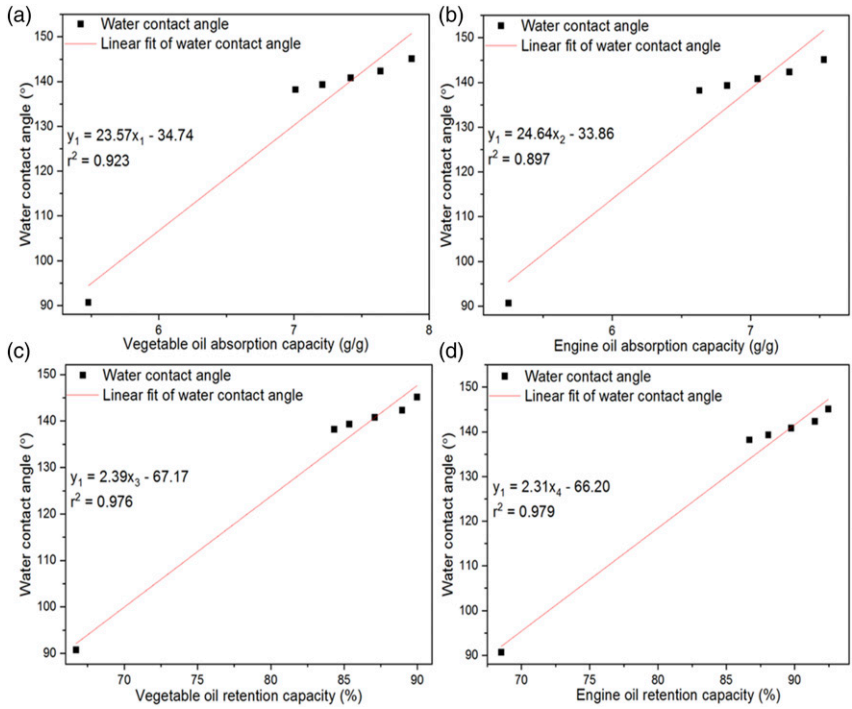

Figure 7. The linear fit curve of water contact angle, oil absorption capacity (a, b), and retention capacity (c, d).

with a higher water contact angle had a greater potential for oil absorption and retention capacity. Moreover, there were interesting relationships among water contact angle, oil absorption capacity, and oil retention capacity from 86 ± 1.14° to 142 ± 0.84°, where the r-square correlation of linear fitting was (0.923 and 0.976) and (0.897 and 0.979) for vegetable oil and engine oil, individually. The slope and the intercept of the curves were (23.57 and −34.74) and (2.29 and −67.17) for vegetable oil, and (24.64 and −33.86) and (2.31 and −66.20) for engine oil, respectively. Therefore, the relationships among water contact angle, oil absorption capacity, and oil retention capacity were articulated by equations (4)–(7).

$$y_1 = 23.57x_1 - 34.74 \tag{4}$$

$$y_1 = 24.64x_2 - 33.86 \tag{5}$$

$$y_1 = 2.39x_3 - 67.17 \tag{6}$$

$$y_1 = 2.31x_4 - 66.20 \tag{7}$$

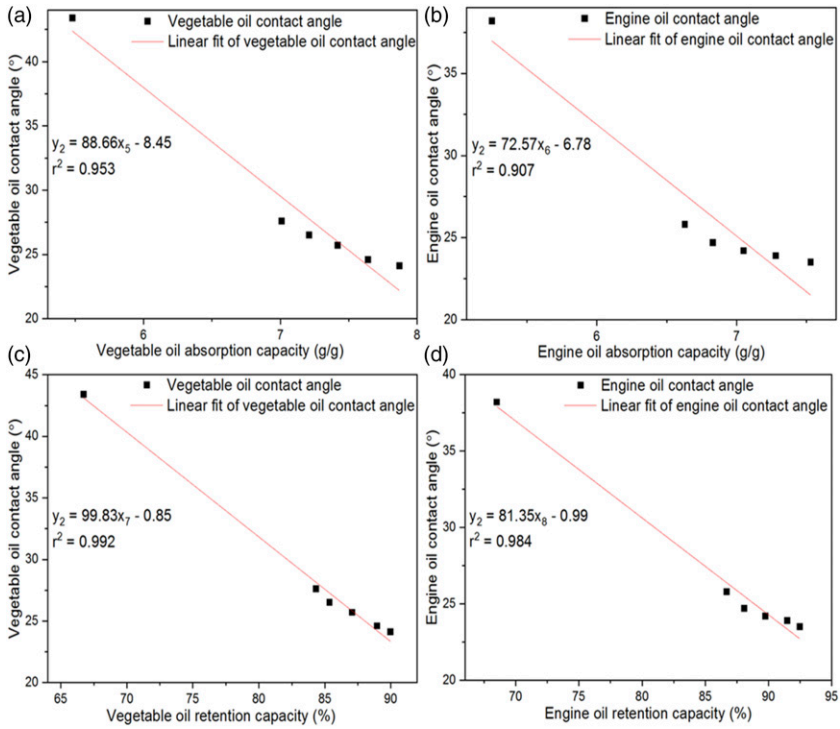

Figure 8. The linear fit curve of oil contact angle, oil absorption capacity (a, b), and retention capacity (c, d).

where y_1 is the water contact angle, (x_1 and x_2) are the vegetable oil and engine oil absorption capacity, and (x_3 and x_4) are the vegetable oil and engine oil retention capacity.

Generally, the greater the water contact angle, the higher the oil absorption capacity and oil retention capacity of the 3D WKSFs. When three factors, namely, water contact angle, oil absorption capacity, and oil retention capacity were compared in this research, the results predicted that water contact angle would be the most significant factor in oil absorption and retention capacity.

The relationships among oil contact angle, oil absorption, and retention capacity

The oil absorption and retention capacity capability of 3D WKSFs were also expressed by the oil contact angle. The oil contact angle, oil absorption capacity, and oil retention capacity curves had been shown in Figure 8 by decreasing the direction of the oil contact angle of the three untreated and treated 3D WKSFs. Once the vegetable oil and engine oil contact angle ranged from (43.4 ± 0.68° to 24.1 ± 0.33°) and (38.2 ± 0.59° to 23.5 ± 0.26°), the oil absorption capacity and oil retention capacity of untreated and treated 3D spacer fabrics transformed from (5.48 ± 0.18 g/g to 7.87 ± 0.09 g/g) and (66.72 ± 1.19% to 89.98 ± 0.79%) for vegetable oil and

(5.25 ± 0.15 g/g to 7.53 ± 0.06 g/g) and (68.52 ± 1.11% to 92.48 ± 0.56%) for engine oil, respectively. This directed that 3D WKSFs with a lower oil contact angle had a higher oil absorption capacity and oil retention capacity. Further, there were progressive relationships among oil contact angle, oil absorption capacity, and oil retention capacity from (43.4 ± 0.68° to 24.1 ± 0.33°) and (38.2 ± 0.59° to 23.5 ± 0.26°), where the r-square correlation of linear fitting was (0.953 and 0.992) and (0.907 and 0.984) for vegetable oil and engine oil, individually. The slope and the intercept of the curves were (88.66 and −8.45) and (99.83 and −0.85) for vegetable oil, and (72.57 and −6.78) and (81.35 and −0.99) for engine oil, consistently. Thus, the relationships among oil contact angle, oil absorption capacity, and oil retention capacity were computed by equations (8)–(11).

$$y_2 = 88.66x_5 - 8.45 \tag{8}$$

$$y_2 = 72.57x_6 - 6.78 \tag{9}$$

$$y_2 = 99.83x_7 - 0.85 \tag{10}$$

$$y_2 = 81.35x_8 - 0.99 \tag{11}$$

where y_2 is the oil contact angle, (x_5 and x_6) are the vegetable oil and engine oil absorption capacity, and (x_7 and x_8) are the vegetable oil and engine oil retention capacity.

Likewise, the lower the oil contact angle, the higher the oil absorption capacity and oil retention capacity of the 3D WKSFs. While relating these factors, like oil contact angle, oil absorption capacity, and oil retention capacity, the consequences expected that oil contact angle was another key inducing factor in oil absorption and retention capacity.

The reusability cycles of the vegetable and engine oil absorption of sorbents

The oil absorption capacity increased with the increase of 3D WKSF sorbents' pore diameter, pore volume, and nanoporous silica aerogel add-on %. Consequently, a higher pore diameter offered more free space to absorb the oil. In an oil spill cleanup operation, the oil was extracted from the sorbents by a simple manual hand squeezing repeatedly without losing its enormous hydrophobicity, and the sorbents were subsequently employed multiple times. Furthermore, after a simple wash with a volatile liquid and drying at room temperature, the fabric sorbents were reused (see, Figure S2, Supplementary Supporting file). Besides, Figure 9 showed how the first five squeezing cycles resulted in noticeable reductions in oil absorption capacity. After that, the oil absorption capacity of the fabric sorbents seemed to stabilize. Both vegetable oil and engine oil absorption capacities followed a similar pattern. The irreversible deformation of the spacer fabric sorbents' squeezing was considered to be the cause of the lower oil absorption capacity, which occurred mainly during early cycles.

Statistical analysis of 3D weft-knitted spacer fabrics

For eight different variables (specific surface area (SSA), pore diameter (PD), pore volume (PV), surface roughness (SR), water contact angle (WCA), oil contact angle (OCA), oil

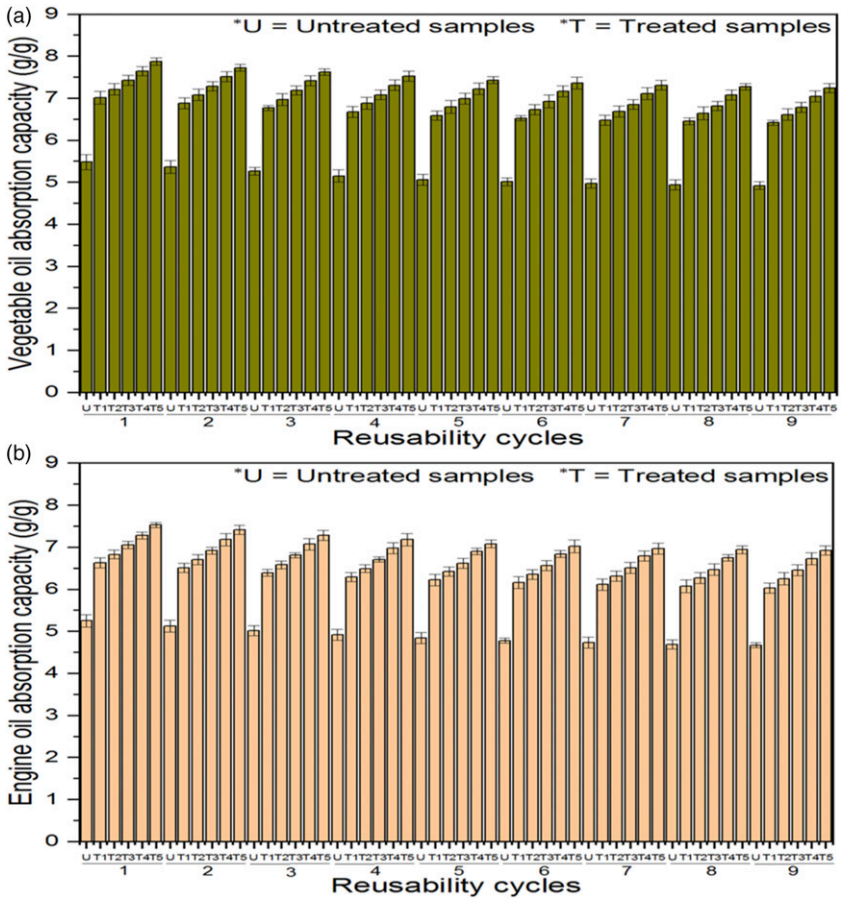

Figure 9. Reusability cycles of (a) vegetable oil and (b) engine oil absorption capacities.

absorption capacity (OAC), and oil retention capacity (ORC) of vegetable oil (VO) and engine oil (EO)), a statistical two-tailed pairwise t-test was studied between untreated samples (UTS) and treated samples (TS) of 3D WKSFs, as listed in Table 6. In all eight variables, there were significant variations between UTS and TS (5% statistically significant level where $p < 0.05$), i.e., specific surface area: $t = -187.25$, $p = 0.000$; surface roughness: $t = -16.54$, $p = 0.000$; pore diameter: $t = -49.06$, $p = 0.000$; pore volume: $t = -24.13$, $p = 0.000$; water contact angle: $t = -87.871$, $p = 0.000$; oil contact angle: (VO: $t = 62.802$, $p = 0.000$, EO: $t = 70.535$, $p = 0.000$); oil absorption capacity: (VO: $t = -19.663$, $p = 0.000$; EO: $t = -20.672$, $p = 0.000$); oil retention capacity: (VO: $t = -37.862$, $p = 0.000$; EO: $t = -41.362$, $p = 0.000$). The t-test exhibited that the UTS produced better outcomes in all autonomous variables. Moreover, all the TS outperformed than the UTS in terms of

Table 6. The statistical analysis of untreated and treated 3D WKSFs.

Test methods		Samples	No	Mean	Std. deviation	Std. error mean
SSA		UTS	15	1.131	0.017	0.004
		TS	15	5.328	0.084	0.022
SR		UTS	15	0.815	0.015	0.003
		TS	15	1.087	0.063	0.016
PD		UTS	15	3.055	0.030	0.007
		TS	15	3.877	0.056	0.014
PV		UTS	15	0.002	0.0001	0.00002
		TS	15	0.013	0.0018	0.00046
WCA		UTS	25	90.70	1.253	0.251
		TS	25	141.14	2.574	0.515
	VOCA	UTS	25	43.40	0.629	0.126
OCA		TS	25	25.70	1.351	0.270
	EOCA	UTS	25	38.20	0.544	0.109
		TS	25	24.42	0.867	0.173
	VO	UTS	15	5.48	0.1549	0.040
OAC		TS	15	7.43	0.3306	0.085
	EO	UTS	15	5.25	0.1272	0.033
		TS	15	7.06	0.3385	0.087
	VO	UTS	25	66.72	1.0886	0.218
ORC		TS	25	87.14	2.3376	0.468
	EO	UTS	25	68.52	1.0133	0.203
		TS	25	89.70	2.3158	0.463

Methods		t	Sig. (2-tailed) *p*-value	Mean diff	Std. error diff	95% confidence interval of the difference	
						Lower	Upper
SSA		−187.25	0.000	−4.196	0.0224	−4.244	−4.148
SR		−16.54	0.000	−0.271	0.0165	−0.307	−0.237
PD		−49.06	0.000	−0.822	0.0168	−0.858	−0.786
PV		−24.13	0.000	−0.011	0.0005	−0.012	−0.010
WCA		−87.871	0.000	−50.440	0.5740	−51.624	−49.255
OCA	VOCA	62.802	0.000	17.70	0.2818	17.118	18.282
	EOCA	70.535	0.000	13.784	0.1954	13.381	14.187
OAC	VO	−19.663	0.000	−1.951	0.0992	−2.163	−1.738
	EO	−20.672	0.000	−1.811	0.0876	−1.996	−1.623
ORC	VO	−37.862	0.000	−20.420	0.5393	−21.533	−19.307
	EO	−41.362	0.000	−21.176	0.5120	−22.233	−20.119

Paired sample t-test (paired differences).

hydrophobic and oleophilic properties with tremendous reusability, as the chemical composition of SiO_2 aerogels had the greatest impact on the surfaces of the 3D WKSFs.

Conclusion

In the current research, untreated samples (UTS) and treated samples (TS 1, TS 2, TS 3, TS 4, and TS 5) with nanoporous silica aerogels (SAs) of 3D weft-knitted spacer fabrics (WKSFs) were studied for hydrophobic, oleophilic, and reusability properties by using the sol-gel method. The performance investigation of eight different variables of WKSFs was statistically significant ($p = 0.000$ at the 0.05 level). Associating all treated samples, TS five having the greater silica aerogel add-on %, had the best outcomes in terms of characteristics. Hence, the specific surface area, surface roughness, pore diameter, and pore volume enhanced significantly, and that was (from 1.131 ± 0.02 m^2g^{-1} to 5.435 ± 0.03 m^2g^{-1}), (from 0.82 ± 0.02 μm to 1.16 ± 0.01 μm), (from 3.055 ± 0.04 Nm to 3.945 ± 0.02 Nm), and (from 0.0015 ± 0.0001 cm^3g^{-1} to 0.0150 ± 0.0002 cm^3g^{-1}), respectively, thus, indicating the tremendous hydrophobic and oleophilic properties of all TS. The WCA promoted from $90.7 \pm 1.37°$ to $145.1 \pm 0.42°$, allowing them to be utilized as an excellent water-repelling or hydrophobic resource. In contrast, the surface energy decreased from 34.33 ± 0.60 $mN.m^{-1}$ to 20.96 ± 0.19 $mN.m^{-1}$, and the OCA declined (from $43.4 \pm 0.69°$ to $24.1 \pm 0.32°$) and (from $38.2 \pm 0.60°$ to $23.5 \pm 0.25°$) for both vegetable oil and engine oil, individually, letting them to be exploited as a unique oil-absorbing or oleophilic resource. The oil absorption capacity of TS enhanced (from 5.48 ± 0.18 g/g to 7.87 ± 0.09 g/g) and (from 5.25 ± 0.15 g/g to 7.53 ± 0.06 g/g) for vegetable oil and engine oil, respectively. The absorption capacity of vegetable oil was superior to that of engine oil. Similarly, the oil retention capacity of TS upgraded (from $66.72 \pm 1.19\%$ to $89.98 \pm 0.79\%$) for vegetable oil and (from $68.52 \pm 1.11\%$ to $92.48 \pm 0.56\%$) for engine oil, individually. Conversely, the outcomes of the engine oil retention capacity were greater than the vegetable oil. Therefore, the excellent hydrophobicity and oleophilicity with notable reusability of 3D WKSFs were developed greatly, making them suitable for industrial uses such as potential water-repelling (hydrophobic) materials, oil-absorbing (oleophilic) sorbents, and protecting resources. Besides, the treated 3D WKSFs might be used in harsher conditions by changing aspects of both spacer fabrics and silica aerogels.

Declaration of conflicting interests

The author(s) declared no potential conflicts of interest with respect to the research, authorship, and/or publication of this article.

Funding

The author(s) disclosed receipt of the following financial support for the research, authorship, and/or publication of this article: This work was financially supported by the Shanghai Natural Science Foundation of Shanghai Municipal Science and Technology Commission (20ZR1400600), and the Fundamental Research Funds for the Central Universities (2232021G-06), and the project was

funded by Shanghai Frontier Science Research Center for Modern Textiles, Donghua University, China.

ORCID iD

Syed Rashedul Islam https://orcid.org/0000-0002-8784-426X

Supplemental material

Supplement material for this article is available in online.

References

1. Bayık GD and Altın A. Conversion of an industrial waste to an oil sorbent by coupling with functional silanes. *J Clean Prod* 2018; 196: 1052–1064.
2. Bayık GD and Altın A. Production of sorbent from paper industry solid waste for oil spill cleanup. *Mar Pollution Bulletin* 2017; 125: 341–349.
3. Wang G, Sun Q, Zhang Y, et al. Sorption and regeneration of magnetic exfoliated graphite as a new sorbent for oil pollution. *Desalination* 2010; 263: 183–188.
4. Bai X, Shen Y, Tian H, et al. Facile fabrication of superhydrophobic wood slice for effective water-in-oil emulsion separation. *Separat Purif Technol* 2019; 210: 402–408.
5. Yang M, Chen Z, Liu T, et al. Ultralight and robustly compressible silica aerogel enhanced by AC/C sponge with high oil/water separation. *J Porous Mater* 2022; 29: 523–530.
6. Wang Z, Saleem J, Barford JP, et al. Preparation and characterization of modified rice husks by biological delignification and acetylation for oil spill cleanup. *Environ Technol* 2020; 41: 1980–1991.
7. Ren Y, Guo J, Lu Q, et al. Polypropylene nonwoven fabric@ poly (ionic liquid) s for switchable oil/water separation, dye absorption, and antibacterial applications. *ChemSusChem* 2018; 11: 1092–1098.
8. Zareei Pour F, Sabzehmeidani MM, Karimi H, et al. Superhydrophobic–superoleophilic electrospun nanofibrous membrane modified by the chemical vapor deposition of dimethyl dichlorosilane for efficient oil–water separation. *J Appl Polym Sci* 2019; 136: 47621.
9. Rajan PS, Gopinath KP, Arun J, et al. Hydrothermal liquefaction of Scenedesmus abundans biomass spent for sorption of petroleum residues from wastewater and studies on recycling of post hydrothermal liquefaction wastewater. *Bioresour Technology* 2019; 283: 36–44.
10. Thilagavathi G and Das D. Oil sorption and retention capacities of thermally-bonded hybrid nonwovens prepared from cotton, kapok, milkweed and polypropylene fibers. *J Environmental Management* 2018; 219: 340–349.
11. Pawar AA and Kim H. Sustainable, hydrophobic, and reusable paper waste aerogel as an effective and versatile oil absorbent. *J Environ Chem Eng* 2022; 2(10): 107356.
12. Wu J, Wang N, Wang L, et al. Electrospun porous structure fibrous film with high oil adsorption capacity. *ACS Applied Materials Interfaces* 2012; 4: 3207–3212.
13. Ifelebuegu AO, Lale EE, Mbanaso FU, et al. Facile fabrication of recyclable, superhydrophobic, and oleophilic sorbent from waste cigarette filters for the sequestration of oil pollutants from an aqueous environment. *Processes* 2018; 6: 140.

14. Davoodi SM, Taheran M, Brar SK, et al. Hydrophobic dolomite sorbent for oil spill clean-ups: Kinetic modeling and isotherm study. *Fuel* 2019; 251: 57–72.
15. Li M, Bian C, Yang G, et al. Facile fabrication of water-based and non-fluorinated super-hydrophobic sponge for efficient separation of immiscible oil/water mixture and water-in-oil emulsion. *Chem Eng J* 2019; 368: 350–358.
16. Alassod A, Islam SR, Farooq A, et al. Fabrication of polypropylene/lignin blend sponges via thermally induced phase separation for the removal of oil from contaminated water. *SN Appl Sci* 2020; 2: 1–10.
17. Liu Y, Tian J, Duan Z, et al. Effect of oil surface activity on oil absorption behavior of potato strips during frying process. *Food Chem* 2021; 365: 130427.
18. Alassod A, Tina H, Islam SR, et al. Using polypropylene needle punch nonwoven sorbents as the interceptor for oil in static and dynamic water experiments. *Environ Technol* 2021; 1(16): 0959–3330.
19. Alassod A, Gibril M, Islam SR, et al. Polypropylene/lignin blend monoliths used as sorbent in oil spill cleanup. *Heliyon* 2020; 6: e04591.
20. Olga VR, Darina VI, Alexandr AI, et al. Cleanup of water surface from oil spills using natural sorbent materials. *Proced Chem* 2014; 10: 145–150.
21. Liu F, Ma M, Zang D, et al. Fabrication of superhydrophobic/superoleophilic cotton for application in the field of water/oil separation. *Carbohydr Polymers* 2014; 103: 480–487.
22. Islam SR, Yousif AHD, et al. Using various concentrations of SiO2 aerogel for oil wicking, spreading, and interception tests of 3D weft-knitted spacer fabrics. *The Journal of the Textile Institute* 2022; 10.1080/00405000.2022.2110027:1754-2340.
23. Janqamsari Y, Ashjari M and Niazi Z. Carbon nanotube promoted porous nanocomposite based on PVA and recycled PET fibers for efficient oil spills cleanup applications. *Chem Pap* 2021; 75: 3443–3456.
24. Saleem J, Riaz MA and Gordon M. Oil sorbents from plastic wastes and polymers: A review. *J Hazardous Materials* 2018; 341: 424–437.
25. Duman O, Diker CÖ, Uğurlu H, et al. Highly hydrophobic and superoleophilic agar/PVA aerogels for selective removal of oily substances from water. *Carbohydr Polym* 2022; 286: 119275.
26. Renuka S, Rengasamy R and Das D. Studies on needle-punched natural and polypropylene fiber nonwovens as oil sorbents. *J Ind Textiles* 2016; 46: 1121–1143.
27. Guo M, Liang H, Luo Z, et al. Study on melt-blown processing, web structure of polypropylene nonwovens and its BTX adsorption. *Fibers Polym* 2016; 17: 257–265.
28. Xu M, Bian J, Han C, et al. Hydrophobic modification of polypropylene/starch blend foams through tailoring cell diameter for oil-spill cleanup. *RSC Advances* 2016; 6: 82088–82095.
29. Vert M. Aliphatic polyesters: great degradable polymers that cannot do everything. *Biomacromolecules* 2005; 6: 538–546.
30. Carosio F, Di Blasio A, Cuttica F, et al. Flame retardancy of polyester and polyester–cotton blends treated with caseins. *Ind Eng Chem Res* 2014; 53: 3917–3923.
31. Divya V and Sarkar N. Plastic mulch pollution and introduction of biodegradable plastic mulches—a review. *Agric Rev* 2019; 40: 314–318.
32. Padmanabhan SK, Protopapa C and Licciulli A. Stiff and tough hydrophobic cellulose-silica aerogels from bacterial cellulose and fumed silica. *Process Biochem* 2021; 103: 31–38.

33. Cok SS, Koc F and Gizli N. Lightweight and highly hydrophobic silica aerogels dried in ambient pressure for an efficient oil/organic solvent adsorption. *J Hazard Mater* 2021; 408: 124858.
34. Yu X, Xiong Y, Li Z, et al. Preparation and characterization of tris (trimethylsiloxy) silyl modified polyurethane acrylates and their application in textile treatment. *Polymers* 2020; 12: 1629.
35. Zheng H, Shan H, Bai Y, et al. Assembly of silica aerogels within silica nanofibers: towards a super-insulating flexible hybrid aerogel membrane. *RSC Advances* 2015; 5: 91813–91820.
36. Thakkar SV, Pinna A, Carbonaro CM, et al. Performance of oil sorbents based on reduced graphene oxide–silica composite aerogels. *J Environ Chem Eng* 2020; 8: 103632.
37. Wu D, Fu R, Sun Z, et al. Low-density organic and carbon aerogels from the sol–gel polymerization of phenol with formaldehyde. *J Non-crystalline Sol* 2005; 351: 915–921.
38. Rao AV, Hegde ND and Hirashima H. Absorption and desorption of organic liquids in elastic superhydrophobic silica aerogels. *J Colloid Interface Science* 2007; 305: 124–132.
39. Choi S-J, Kwon T-H, Im H, et al. A polydimethylsiloxane (PDMS) sponge for the selective absorption of oil from water. *ACS Applied Materials Interfaces* 2011; 3: 4552–4556.
40. Gurav JL, Rao AV, Nadargi D, et al. Ambient pressure dried TEOS-based silica aerogels: good absorbents of organic liquids. *J Materials Science* 2010; 45: 503–510.
41. Yu Y, Wu X, Guo D, et al. Preparation of flexible, hydrophobic, and oleophilic silica aerogels based on a methyltriethoxysilane precursor. *J Mater Sci* 2014; 49: 7715–7722.
42. Wang C, Yao T, Wu J, et al. Facile approach in fabricating superhydrophobic and superoleophilic surface for water and oil mixture separation. *ACS Applied Materials Interfaces* 2009; 1: 2613–2617.
43. Gu J, Xiao P, Chen P, et al. Functionalization of biodegradable PLA nonwoven fabric as superoleophilic and superhydrophobic material for efficient oil absorption and oil/water separation. *ACS Applied Materials Interfaces* 2017; 9: 5968–5973.
44. Sun M, Zhao S, Wei W, et al. Polyacrylamide-modified polyester fabric with easy-cleaning for efficient oil/water separation. *AATCC J Res* 2018; 5: 1–6.
45. Wang G and Uyama H. Facile synthesis of flexible macroporous polypropylene sponges for separation of oil and water. *Scientific Reports* 2016; 6: 1–6.
46. Wang G, Peng L, Yu B, et al. Hierarchically porous sponge for oily water treatment: facile fabrication by combination of particulate templates and thermally induced phase separation method. *J Industrial Engineering Chemistry* 2018; 62: 192–196.
47. Alassod A, Khalaji MS, Islam SR, et al. Polypropylene-chitosan sponges prepared via thermal induce phase separation used as sorbents for oil spills cleanup. *Polym Bull* 2022; 116: 1436–2449.
48. Anjum AS, Ali M, Sun KC, et al. Self-assembled nanomanipulation of silica nanoparticles enable mechanochemically robust super hydrophobic and oleophilic textile. *J Colloid Interface Science* 2020; 563: 62–73.
49. He J, Zhao H, Li X, et al. Superelastic and superhydrophobic bacterial cellulose/silica aerogels with hierarchical cellular structure for oil absorption and recovery. *J Hazardous Materials* 2018; 346: 199–207.
50. Chen C, Du Z, Yu W, et al. Analysis of physical properties and structure design of weft-knitted spacer fabric with high porosity. *Textile Res J* 2018; 88: 59–68.

51. Islam SR, Yu W and Naveed T. Influence of silica aerogels on fabric structural feature for thermal isolation properties of weft-knitted spacer fabrics. *J Engineered Fibers Fabrics* 2019; 14: 1558925019866446.
52. Liu Y and Hu H. Compression property and air permeability of weft-knitted spacer fabrics. *J Textile Inst* 2011; 102: 366–372.
53. Yang Y and Hu H. Spacer fabric-based exuding wound dressing–Part I: Structural design, fabrication and property evaluation of spacer fabrics. *Textile Res J* 2017; 87: 1469–1480.
54. Arumugam V, Mishra R, Militky J, et al. Investigation on thermo-physiological and compression characteristics of weft-knitted 3D spacer fabrics. *J Textile Inst* 2017; 108: 1095–1105.
55. Islam SR, Patoary MK, Farooq A, et al. 3D weft-knitted spacer fabrics (WKSFs) coated with silica aerogels as oil intercepting sorbents for use in static and dynamic water tests. *Ind Crops Prod* 2022; 186: 115169.
56. Ding F and Gao M. Pore wettability for enhanced oil recovery, contaminant adsorption and oil/water separation: A review. *Adv Colloid Interf Sci* 2021; 289: 102377.
57. Davies A and Williams J. The use of spacer fabrics for absorbent medical applications. *J Fiber Bioeng Inform* 2009; 1: 321–330.
58. Islam SR and Rakib MAN. Mechanical properties of weft-Knitted spacer fabrics integrated with silica aerogels. *J Donghua Univ (English Edition)* 2020; 36(6): 559–563.
59. Zhang M, Wang S, Wang C, et al. A facile method to fabricate superhydrophobic cotton fabrics. *Appl Surf Sci* 2012; 261: 561–566.
60. Xiu Y, Hess DW and Wong C. UV and thermally stable superhydrophobic coatings from sol–gel processing. *J Colloid Interface Science* 2008; 326: 465–470.
61. Bae GY, Jang J, Jeong YG, et al. Superhydrophobic PLA fabrics prepared by UV photografting of hydrophobic silica particles possessing vinyl groups. *J Colloid Interface Science* 2010; 344: 584–587.
62. Rao AV, Latthe SS, Nadargi DY, et al. Preparation of MTMS based transparent superhydrophobic silica films by sol–gel method. *J Colloid Interface Science* 2009; 332: 484–490.
63. Islam SR, Alassod A, Naveed T, et al. The study of hydrophobicity and oleophilicity of 3D weft-knitted spacer fabrics integrated with silica aerogels. *J Ind Textiles* 2021; 15280837211029048: 0837–1528.
64. Latthe SS, Hirashima H and Rao AV. TEOS based water repellent silica films obtained by a co-precursor sol–gel method. *Smart Materials Structures* 2009; 18: 095017.
65. Latthe SS, Nadargi DY and Rao AV. TMOS based water repellent silica thin films by co-precursor method using TMES as a hydrophobic agent. *Appl Surf Sci* 2009; 255: 3600–3604.
66. Latthe SS, Imai H, Ganesan V, et al. Superhydrophobic silica films by sol–gel co-precursor method. *Appl Surf Sci* 2009; 256: 217–222.
67. Li F, Xing Y and Ding X. Silica xerogel coating on the surface of natural and synthetic fabrics. *Surf Coat Technol* 2008; 202: 4721–4727.
68. Li M, Jiang H and Xu D. Preparation of sponge-reinforced silica aerogels from tetraethoxysilane and methyltrimethoxysilane for oil/water separation. *Mater Res Express* 2018; 5: 045003.
69. He S, Cheng X, Li Z, et al. Green and facile synthesis of sponge-reinforced silica aerogel and its pumping application for oil absorption. *J Materials Science* 2016; 51: 1292–1301.

70. Dong T, Xu G and Wang F. Oil spill cleanup by structured natural sorbents made from cattail fibers. *Ind Crops Prod* 2015; 76: 25–33.
71. Krüger R, Bockmeyer MJ, Dutschke A, et al. Continuous sol–gel coating of ceramic multifilaments: evaluation of fiber bridging by three-point bending test. *J Am Ceram Soc* 2006; 89: 2080–2088.
72. Alassod A, Islam SR, Khalaji MS, et al. Polypropylene/lignin/POSS nanocomposites: thermal and wettability properties, application in water remediation. *Materials* 2021; 14: 3950.
73. Karan CP, Rengasamy R and Das D. Oil spill cleanup by structured fibre assembly. *Indian J Fibre Text Res* 2011; 36(2): 190–200.